IL NUOVO CIMENTO Vol. 32 C, N. 2 Marzo-Aprile 2009
DOI 10.1393/ncc/i2009-10383-x

Colloquia: CSFI 2008

Unsteady interactional aerodynamics of a helicopter configuration

M. Biava

Dipartimento di Ingegneria Aerospaziale, Politecnico di Milano - Milano, Italy

(ricevuto il 15 Maggio 2009; pubblicato online il 3 Settembre 2009)

Summary. — In this paper we present the aerodynamic simulation of a complex rotor/fuselage configuration performed with the CFD solver ROSITA (ROtorcraft Software ITAly), developed at the Aerospace Department of the Politecnico di Milano.

PACS 47.10.ad – Navier-Stokes equations.
PACS 47.11.-j – Computational methods in fluid dynamics.
PACS 47.11.Df – Finite volume methods.

1. – Introduction

We present the aerodynamic analysis of a complex rotor/fuselage configuration performed with the CFD solver ROSITA (ROtorcraft Software ITAly), developed at the Aerospace Department of the Politecnico di Milano. The configuration considered for the simulation consists of the NH90 helicopter fuselage and of the four-bladed ONERA rotor with 7AD1 blades, inserted into the DNW LLF wind tunnel. The flight conditions are those of a typical cruise flight. Plots of the computed flow field and of the integrated loads will be shown. The analysis of the numerical solution demonstrates, at least qualitatively, the capability of the ROSITA solver to capture the fundamental interactional phenomena that characterize a rotor/fuselage configuration.

2. – Description of the CFD code

The ROSITA solver numerically integrates the unsteady RANS equations coupled with the one-equation turbulence model of Spalart-Allmaras. The equations are discretized in space by means of a cell-centred finite-volume implementation of the Roe's scheme. A high-resolution scheme is obtained through the use of MUSCL extrapolation supplemented with a total variation diminishing (TVD) limiter to ensure monotone solutions. Time advancement is carried out with a dual-time formulation. A 2nd-order backward differentiation formula was applied to approximate the time derivative and a fully unfactored implicit scheme is used in pseudo-time.

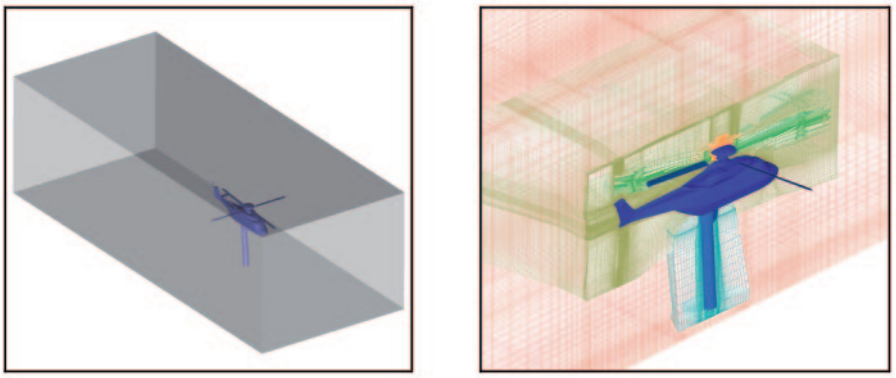

Fig. 1. – GOAHEAD model in the DNW LLF wind tunnel test section (left) and partial view of the computational grid (right).

ROSITA can deal with bodies in relative motion (the rotor blades, for instance) thanks to the Chimera technique, which is an algorithm for computing the connectivity between multiple overlapping grids, possibly moving and deforming.

The CFD solver is capable of running in parallel on workstation clusters. The parallel code is based on the message passing programming paradigm and the parallelization strategy is to distribute the grid blocks among the available processors. Moreover, to attain an optimal load balancing, the the grid blocks may be further partitioned (automatically) into smaller ones by the solver.

3. – Analysis of the NH90 fuselage/7AD rotor configuration

The presented numerical simulation considers the full helicopter configuration tested in the closed $6 \times 8\,\mathrm{m}$ test section of the DNW LLF wind tunnel during the Common European Project GOAHEAD. The configuration under investigation is a Mach scaled model similar to a modern transport helicopter consisting of a four-bladed main rotor with ONERA 7AD blades and the NH90 fuselage (see fig. 1). The model has length $L = 4.15\,\mathrm{m}$ and rotor radius $R = 2.10\,\mathrm{m}$.

The Chimera grid system for the numerical simulation is made up of 8 component grids for a total of 144 blocks and $1.5 \cdot 10^7$ grid cells (fig. 1). The selected test case for the rotor/fuselage configuration refers to a typical cruise flight condition. The characteristic flight parameters are reported in the following table I.

TABLE I. – *Flight parameters.*

Free-stream Mach number	M_∞	0.204
Reynolds number	$Re = \frac{V_\infty R}{\nu_\infty}$	9.4×10^6
Fuselage pitch angle	α_F	-2°
Tip Mach number	M_tip	0.617
Fuselage drag coefficient	C_X	0.042
Main rotor thrust coefficient	C_t/σ	0.071
Main rotor power coefficient	C_P/σ	0.0057

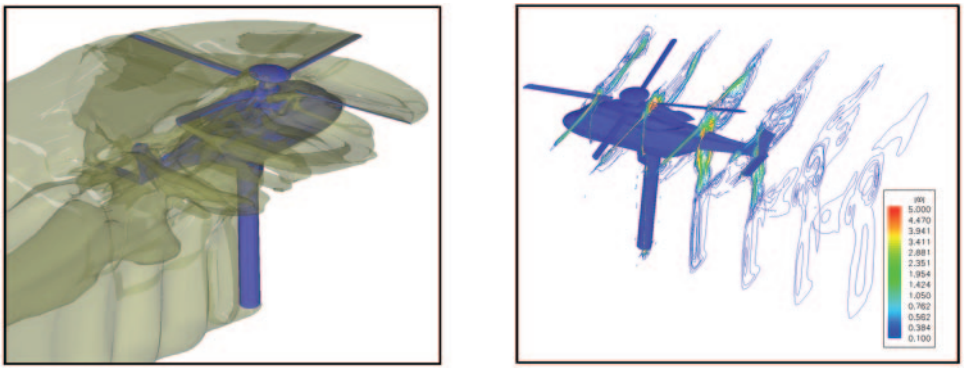

Fig. 2. – Isossurface of the entropy $s = 0.002$, giving a pitcure of the complex vortical structures shed by the rotor and the fuselage (left) and isolines of the vorticity vector modulus $|\boldsymbol{\omega}|$ in correspondence of different $X = \text{const}$ slices of the flowfield (right).

The unsteady RANS equations coupled with the Spalart-Allmaras turbulence model have been solved for 3 complete revolutions of the main rotor, advancing the azimuth angle by 2° at each time step. No-slip adiabatic wall boundary conditions were imposed on all solid surfaces, exception made for the wind tunnel walls, that were instead treated as inviscid walls.

We now turn to the discussion of the numerical results. Figure 2 shows an isossurface of the entropy and indicates that the rotor wake system is already fully developed and that it has been convected sufficiently far downstream so that the solution is nearly periodic after the computed 3 revolutions of the main rotor.

This is confirmed by looking at the temporal history of the forces induced by the rotor wake system on the control surfaces. In fig. 3, for instance, the lateral force coefficient C_Y on the vertical fin is reported, and a nearly periodic variation of the coefficient can be observed for the second and third revolution. It is interesting to observe how the predicted forcing on the vertical fin exhibits the characteristic frequency of 4 cycles per revolution, typical of a four-bladed rotor. A similar behavior can be seen when inspecting the vertical force coefficient C_Z on the horizontal stabilizer, given on the same figure. In this last case, however, the force coefficient exhibits a more irregular variation. This may be justified by inspecting the isolines of the vorticity vector modulus in fig. 2. The figure suggests that the horizontal stabilizer is subject not only to the forcing of rotor wake system, but also to the forcing of vortical structures that detach from the fuselage.

Figure 4 shows the integral curves of the surface stress vector field and the pressure coefficient distribution at the end of the simulation. We can observe that the flow is attached on the blade at $\Psi = 0°$([1]) and on the blade at $\Psi = 90°$, while there is an unexpected separated region on the blade at $\Psi = 180°$, possibly indicating a lack of spatial or temporal resolution. The retreating blade, on the other hand, exhibits a mostly separated flow, expecially in the inboard sections, for $r/R < 0.5$.

From the analysis of the test case presented above, it is clear that, at least qualitatively, the ROSITA CFD solver is capable of predicting the typical interactional phenom-

([1]) The azimuth angle is zero for the blade pointing in the positive X-direction, and is positive for a clockwise rotation of the rotor seen from above. This is a true French rotor.

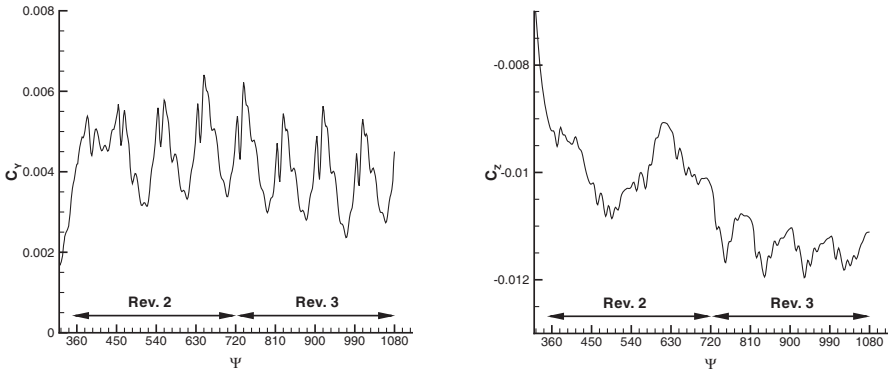

Fig. 3. – Force coefficient C_Y on the vertical fin (left) and force coefficient C_Z on the horizontal stabilizer (right).

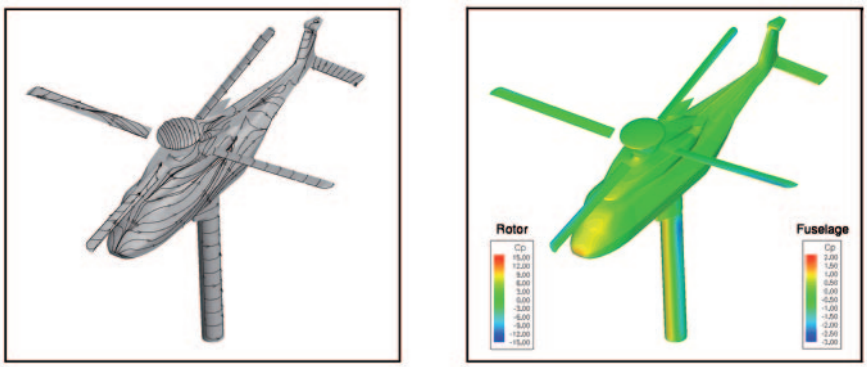

Fig. 4. – Integral curves of the surface stress vector field at $\Psi = 1080^\circ$ (left) and distribution of the pressure coefficient C_p at $\Psi = 1080^\circ$ (right).

ena that characterize a rotor/fuselage configuration. The computed global forces show a satisfactory agreement with those resulting from the trimming procedure. Moreover, the forces acting on the fuselage exhibit the characteristic frequency of the large-scale vortical structures generated by the four-bladed rotor. Separating and recirculating flows are also captured by the numerical solution.

4. – Conclusions

We presented the numerical analysis of the aerodynamic field around a rotor/fuselage configuration in forward flight. Some details about the CFD solver and a brief summary of the simulation parameters were given. Then the computed flow field and the time history of some relevant integrated quantities were shown and discussed. The presented results have demonstrated the capabilities of our CFD solver to perform large-scale simulations of helicopter configurations and to capture the fundamental features of the flow field.

* * *

This work has been partially funded by EC through the GOAHEAD project.